Full Paper
doi.org/10.1002/chem.201905796

Magnetic Properties | *Hot Paper*

Coexistence of Spin–Lattice Relaxation and Phonon-Bottleneck Processes in Gd^{III}–Phthlocyaninato Triple-Decker Complexes under Highly Diluted Conditions

Yoji Horii,*[a] Keiichi Katoh,*[b] Yuji Miyazaki,[c] Marko Damjanović,[d] Tetsu Sato,[b] Liviu Ungur,[e] Liviu F. Chibotaru,[f] Brian K. Breedlove,[b] Motohiro Nakano,[c] Wolfgang Wernsdorfer,[d] and Masahiro Yamashita*[a, b, g]

Abstract: Gd^{3+} complexes have been shown to undergo unusual slow magnetic relaxation processes similar to those of single-molecule magnets (SMMs), even though Gd^{3+} does not exhibit strong magnetic anisotropy. To reveal the origin of the slow magnetic relaxation of Gd^{3+} complexes, we have investigated the magnetic properties and heat capacities of two Gd^{3+}-phthalocyaninato triple-decker complexes, one of which has intramolecular Gd^{3+}–Gd^{3+} interactions and the other does not. It was found that the Gd^{3+}–Gd^{3+} interactions accelerate the magnetic relaxation processes. In addition, magnetically diluted samples, prepared by doping a small amount of the Gd^{3+} complexes into a large amount of diamagnetic Y^{3+} complexes, underwent dual magnetic relaxation processes. A detailed dynamic magnetic analysis revealed that the coexistence of spin–lattice relaxation and phonon-bottleneck processes is the origin of the dual magnetic relaxation processes.

Introduction

Single-molecule magnets (SMMs) are a primary research target in molecular magnetism, and their electronic structures as well as application potential in memory devices and as bits in quantum computers have been extensively studied.[1–5] SMMs with high operating temperatures have been achieved by incorporating strong easy-axis magnetic anisotropy into magnetic metal ions, exploiting the zero-field splitting (ZFS) of transition-metal complexes and/or ligand-field splitting (LFS) of lanthanoid ions.[6–12] Distinct magnetic anisotropy in SMMs induces an activation energy barrier (ΔE) between up- and down-spin states, trapping the polarized spin on one side of the double-well potential. Recently, SMM-like slow magnetic relaxation processes, which can be indirectly observed through ac magnetic susceptibility measurements at ac frequencies below around 1 kHz, have been observed for metal complexes, even in the absence of distinct easy-axis magnetic anisotropy. It has been reported that several kinds of octahedral Co^{2+} mononuclear complexes showing easy-plane magnetic anisotropy undergo slow magnetic relaxation processes.[13–15] Gómez-Coca et al. suggested that these magnetic relaxation processes are due to spin–lattice relaxations, that is, direct and Raman processes between ground-state doublets.[14] In addition, the magnetic properties of 3d[16–18] and 4d[19] metal complexes with isotropic $S = 1/2$, which do not undergo ZFS, have

[a] *Dr. Y. Horii, Prof. Dr. M. Yamashita*
Advanced Institute for Materials Research, Tohoku University
2-1-1 Katahira, Aoba-ku, Sendai 980-8577 (Japan)
E-mail: yoji.horii.c5@tohoku.ac.jp
masahiro.yamashita.c5@tohoku.ac.jp

[b] *Prof. Dr. K. Katoh, T. Sato, Prof. Dr. B. K. Breedlove, Prof. Dr. M. Yamashita*
Department of Chemistry, Graduate School of Science, Tohoku University
6-3 Aramaki-Aza-Aoba, Aoba-ku, Sendai, Miyagi 980-8578 (Japan)
E-mail: keiichi.katoh.b3@tohoku.ac.jp
masahiro.yamashita.c5@tohoku.ac.jp

[c] *Prof. Dr. Y. Miyazaki, Prof. Dr. M. Nakano*
Research Center for Thermal and Entropic Science
Graduate School of Science, Osaka University
1-1 Machikaneyama-cho, Toyonaka, Osaka 560-0043 (Japan)

[d] *Dr. M. Damjanović, Prof. Dr. W. Wernsdorfer*
Institute of Nanotechnology (INT)
Karlsruhe Institute of Technology (KIT), Hermann-von-Helmholtz-Platz 1
76344 Eggenstein-Leopoldshafen (Germany)

[e] *Prof. Dr. L. Ungur*
Department of Chemistry, National University of Singapore
3 Science Drive 3, Singapore 117543 (Singapore)

[f] *Prof. Dr. L. F. Chibotaru*
Theory of Nanomaterials Group, Katholieke Universiteit Leuven
3001 Leuven (Belgium)

[g] *Prof. Dr. M. Yamashita*
School of Materials Science and Engineering
Nankai University, Tianjin 300350 (China)
E-mail: yamasita.m@gmail.com

Supporting information and the ORCID identification number(s) for the author(s) of this article can be found under: https://doi.org/10.1002/chem.201905796.

been extensively studied, and Gd^{3+} complexes have been shown to undergo similar SMM-like slow magnetic relaxation processes.[20–25] The ground-state multiplet of Gd^{3+} is $^8S_{7/2}$ and has no orbital angular momentum. In other words, the magnetic anisotropy of Gd^{3+} is weak. Coronado and Luis and coworkers reported the first examples of fully characterized Gd^{3+} SMMs, which were polyoxometalate (POM) complexes.[21] These complexes have tiny easy-axis magnetic anisotropies because of an admixture of a ground-state doublet ($S_z = \pm 7/2$) and excited states. Due to a very small ΔE (2.2 K), slow magnetic relaxation processes occur below 1 K. In contrast to the Gd^{3+} POM based SMMs, $[phen_2Gd_2(HCOO)_4(HCOO)_{0.96}(NO_3)_{1.04}]$ (phen = 1,10-phenanthroline), reported by Liu et al.,[20] undergoes slow magnetic relaxation up to 5.5 K in a 2.75 kOe static magnetic field. In the case of $Na[Gd(edta)(H_2O)_3]_n \cdot 5H_2O$ (edta = ethylenediaminetetraacetic acid), slow magnetic relaxation has been observed up to 12 K.[23,25] Thermal energy in that temperature range is much larger than the energy scale of ZFS expected for common Gd^{3+} complexes, excluding the Orbach process (common for general SMMs) from the possible mechanism for slow magnetic relaxation.

In this article we report the dynamic magnetic properties of two Gd^{3+}–phthalocyaninato triple-decker complexes, one of which has two Gd^{3+} ions (**GdGd**) and the other has one (**GdY**; Figure 1). **GdGd** shows intramolecular Gd^{3+}–Gd^{3+} interactions, whereas **GdY** shows no intramolecular magnetic interactions. Both complexes undergo SMM-like slow magnetic relaxation processes, with the relaxation times (τ) being dependent on the magnitude of the Gd^{3+}–Gd^{3+} interactions. Furthermore, magnetic dilution by doping a small amount of **GdGd** or **GdY** into diamagnetic **YY** induces dual magnetic relaxation processes. This behavior stems from the coexistence of spin–lattice relaxation (i.e., the Orbach process) and phonon-bottleneck processes.

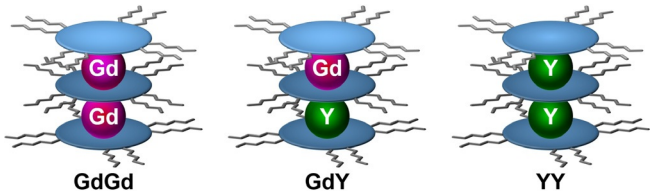

Figure 1. Illustrations of **GdGd**, **GdY**, and **YY**. The blue discs represent obPc ligands.

Results and Discussion

Synthesis and characterization of GdGd and GdY

GdGd was prepared following the method reported by Katoh et al.[26] using H_2(obPc) (obPc = 2,3,9,10,16,17,23,24-octabutoxyphthalocyanine), $[Gd(obPc)_2]$, and $[Gd(CH_3COO)_3] \cdot 4H_2O$. **GdY** and diamagnetic **YY** were synthesized by treating $[Gd(obPc)_2]$ with an excess amount of H_2(obPc) and $[Y(acac)_3]$ (acac = acetylacetonate).[26] Inductively coupled plasma atomic emission spectroscopy (ICP-AES) measurements revealed that the **GdY** sample contained 34.6 mol% of Gd^{3+} and 65.4 mol% of Y^{3+}, consistent with the occupancies of the metal ions determined by single-crystal X-ray diffraction (SXRD) analysis (Gd/Y = 0.33:0.67), which will be discussed later. The peak intensities in the ESI-MS spectra demonstrated that the **GdY** sample contained 49 mol% of **GdY**, 49 mol% of the Y^{3+} analogue **YY**, and 2 mol% of **GdGd**, consistent with the ICP-AES and SXRD results.

GdGd crystallized in the triclinic space group *P*1. The two Gd^{3+} ions in **GdGd** are crystallographically equivalent to each other. The nitrogen atoms of the obPc ligands coordinate to the Gd^{3+} ions to form the sandwich structure shown in Figure 2. Two obPc ligands are twisted by 31.8°, such that the coordination geometry around Gd^{3+} is a distorted square antiprism. The intramolecular Gd^{3+}–Gd^{3+} distance was determined to be 3.538 Å, which is much shorter than the closest intermolecular Gd^{3+}–Gd^{3+} distances (11.003 Å).

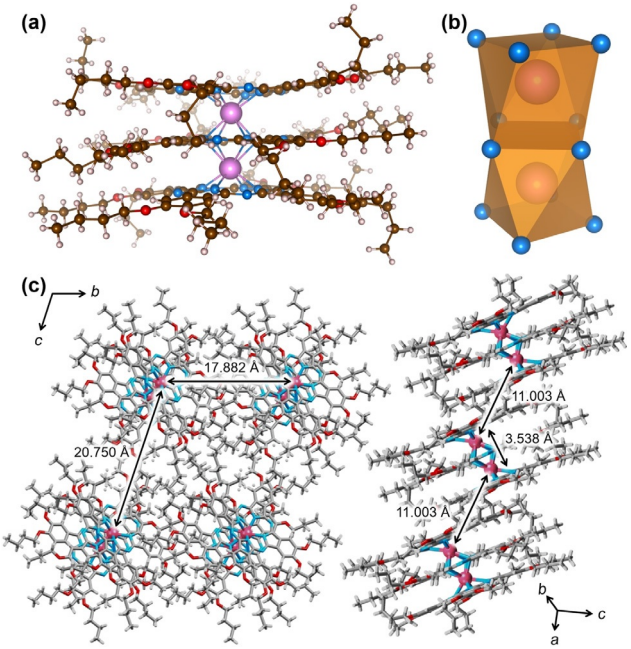

Figure 2. (a) Crystal structure and (b) coordination polyhedron of **GdGd**. Color scheme: pink, Gd; brown, C; red, O; blue, N. (c) Crystal packing of **GdGd**. The numbers in the figures represent Gd^{3+}–Gd^{3+} distances.

GdY crystallized with the same crystal structural parameters as **GdGd** (see Table S1 in the Supporting Information), which indicates that **GdY** and **GdGd** are isostructural. **GdY** contains Gd^{3+} and Y^{3+} ions located in the same positions. In other words, positional disorder occurs at the metal sites. The occupancy ratio of the Gd^{3+} and Y^{3+} ions was determined through SXRD analysis to be 0.33:0.67, which is consistent with the results of the ICP-AES analysis (Gd/Y = 0.35:0.65).

dc Magnetic properties and heat capacities

To determine the magnetic structure of **GdGd**, we conducted dc magnetic and heat capacity measurements. The $\chi_M T$ values for **GdGd** increased markedly at lower temperatures, whereas

those for **GdY** only slightly increased, which indicates that intramolecular ferromagnetic Gd^{3+}–Gd^{3+} interactions are present in **GdGd** (Figure 3a). The small increase in the $\chi_M T$ values for **GdY** is due to the presence of a small amount of magnetic impurities, attributed to **GdGd**.

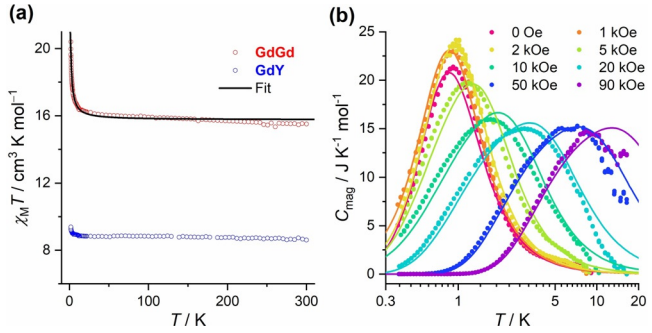

Figure 3. (a) $\chi_M T$ vs. T plots for **GdGd** and **GdY** in a 1 kOe field. (b) C_{mag} vs. T plots for **GdGd**. The data were fitted (solid lines) by using $J_{ex} = 0.0340\ cm^{-1}$ and $D = -0.160\ cm^{-1}$.

The molar magnetic heat capacities (C_{mag}) for **GdGd** were obtained by subtracting the lattice contributions (C_{lat}) from the heat capacities at constant pressure (C_p) acquired on a Quantum Design physical properties measurement system (PPMS). The details of the heat capacity analyses are shown in the Supporting Information. The C_{mag} versus T plots show peaks that shift to higher T with increasing strength of the dc field due to Zeeman effects (Figure 3b). Simultaneous fitting of the $\chi_M T$ versus T plots and C_{mag} versus T plots for **GdGd** was conducted by using the PHI program[27] with the Hamiltonian ($\hat{H}$) given by Equation (1):

$$\hat{H} = -2J_{ex}\boldsymbol{S_1}.\boldsymbol{S_2} + DS_{1z}S_{2z} - g\mu_B\boldsymbol{H_{dc}}(\boldsymbol{S_1} + \boldsymbol{S_2}) \quad (1)$$

in which J_{ex} is the isotropic exchange interaction parameter between Gd^{3+} ions, D is the axial ZFS parameter of Gd^{3+}, $\boldsymbol{S_1}$ and $\boldsymbol{S_2}$ are the spins of the Gd^{3+} ions, S_{1z} and S_{2z} are the z components of $\boldsymbol{S_1}$ and $\boldsymbol{S_2}$, g is the Landé g-factor, $\boldsymbol{H_{dc}}$ is the dc magnetic field and μ_B is the Bohr magneton. The g-factor and the spin quantum numbers (S_1 and S_2) were fixed to 2 and 7/2 on the basis of the ground-state multiplet of the Gd^{3+} ion ($^8S_{7/2}$). Fitting afforded the following values: $J_{ex} = 0.0340\ cm^{-1}$ and $D = -0.160\ cm^{-1}$.

A small negative D value is essential to reproduce the C_{mag} versus T plots. The magnitudes of J_{ex} and D are similar to those obtained for other Gd^{3+} complexes[21,22,24,25,28] and the theoretical values determined by ab initio calculations ($D = -0.101\ cm^{-1}$, see the Supporting Information).[23,29,30] To investigate the effects of intermolecular magnetic interactions, magnetically diluted samples (**GdGd*** and **GdY***) were prepared by doping **GdGd** or **GdY** into an excess amount of diamagnetic **YY**. The ratios of the Gd^{3+} and Y^{3+} ions were determined to be 9.5:90.5 for **GdGd*** and 3.3:96.7 for **GdY***. The $\chi_M T$ versus T plots for **GdGd*** and **GdY*** were similar to those of the undiluted samples. Therefore, the effects of intermolecular interactions on dc magnetic properties are minor compared with the intramolecular interactions (see Figure S5 in the Supporting Information).

ac Magnetic properties

In contrast to the static magnetic properties, the dynamic magnetic properties depend heavily on magnetic dilution. Figure 4a shows the imaginary part of the ac magnetic susceptibility (χ_M'') versus ac frequency (ν) plots for four samples. It is noteworthy that the χ_M'' values of the diluted samples showed a dependence on ν without a dc bias field, which indicates that the magnetic relaxation originates from transitions between ZFS levels (Orbach process) rather than between Zeeman splitting levels (direct process). In contrast, all the reported gadolinium complexes, except for the Gd-POM SMMs, require a dc bias field to show slow magnetic relaxation.[22–25,28] In a field of 200 Oe, the χ_M'' values for **GdGd*** and **GdY*** showed a single peak at around 500 Hz, which we have denoted as a faster relaxation (FR). When the dc field was increased, the FR decreased and slower relaxation (SR) became apparent at around 50 Hz. In contrast, **GdGd** and **GdY** underwent single relaxation processes, which have been attributed to SR, at around 100 and 50 Hz, respectively, over the entire field range. The field dependencies of the τ values for FR and SR (τ_{FR} and τ_{SR}) are shown in Figure 4b. The longest τ_{FR} for **GdGd*** and **GdY*** were observed in a 200 Oe field, which indicates that a weak dc field resolves the degenerate ground-state doublet. In other words, quantum tunneling of magnetization (QTM) was suppressed. Above 200 Oe, τ_{FR} decreased with increasing dc magnetic field, because the applied dc magnetic field enhances the direct process.[31]

Similarly, the decrease in τ_{SR} in a magnetic field above 2 kOe (Figure 4b) is also due to an enhancement of the direct process. The τ_{SR} values decrease in the order **GdY*** > **GdY** > **GdGd*** > **GdGd**, which indicates that τ_{SR} decreases with in-

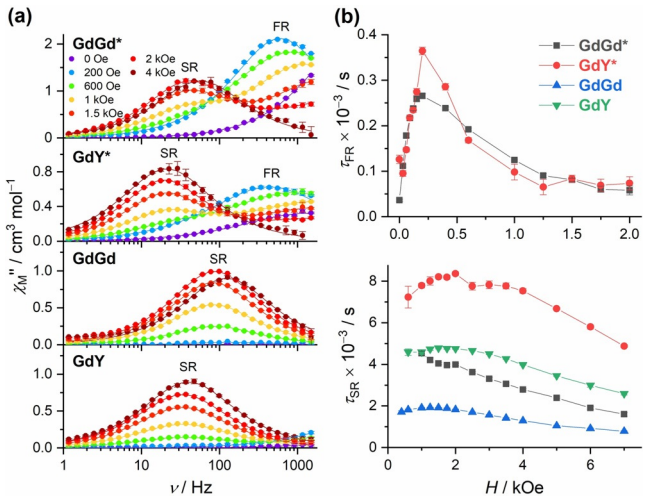

Figure 4. (a) The dc field dependencies of χ_M'' vs. ν plots for **GdGd***, **GdY***, **GdGd**, and **GdY** at 1.85 K. The data were fitted (solid lines) by using the generalized Debye model. (b) Magnetic field dependencies of τ_{FR} and τ_{SR}.

creasing Gd^{3+}–Gd^{3+} interactions. Such interactions increase the number of magnetic states: **GdY** has 8 magnetic states ($2S+1=8$) and **GdGd** has 64 states ($(2S_1+1)\times(2S_2+1)=64$), as shown in Figure S7 in the Supporting Information. Therefore, the number of relaxation pathways for **GdGd** ($64\times63=4032$) is much higher than for **GdY** ($8\times7=56$). In other words, the value of τ for **GdGd** should be smaller than that for **GdY**, which is consistent with the experimental observations. In addition, the Gd^{3+} ions act as a source of fluctuating magnetic field, causing enhanced magnetic relaxations.

To gain further insights into FR and SR, the dependence of T on the ac magnetic susceptibility was investigated in a field of 200 Oe for FR and 2 kOe for SR. Figure 5 shows the Arrhenius plots for τ_{FR} and τ_{SR}. The τ_{FR} data were fitted by using the Arrhenius Equation (2):

$$\tau_{FR} = \tau_0 e^{\Delta E/k_B T} \quad (2)$$

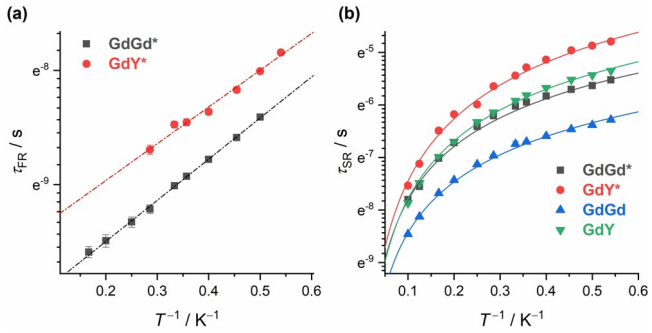

Figure 5. Arrhenius plots for (a) τ_{FR} in a magnetic field of 200 Oe and (b) τ_{SR} in a magnetic field of 2 kOe. The data were fitted by using Equations (2) and (3) (dot-dashed and solid lines, respectively).

in which τ_0 is the frequency factor, ΔE is the activation energy for spin reversal, and k_B is Boltzmann's constant. The optimized ΔE and τ_0 values are presented in Table 1. The ΔE values are close to the magnitude of the ZFS ($|DS_{1z}S_{2z}|\approx2\ cm^{-1}$), which indicates that FR is a result of the Orbach process between the ground and excited ZFS levels, as seen in SMMs. The matrix elements between the magnetic momentum ($\boldsymbol{\mu}$) and magnetic states determined from ab initio calculations, $<S_{1z}|\boldsymbol{\mu}|S_{2z}>$, which correlate with the magnetic relaxation pathway, support magnetic relaxation through excited states.[32] The τ_{SR} data do not obey the Arrhenius relation. Instead, Equation (3) was used to simulate the T dependence of τ_{SR},

$$\tau_{SR} = 1/(AT + BT^2) \quad (3)$$

in which A and B are fitting parameters. Because the value of τ for the direct process is proportional to the inverse of T, AT in Equation (3) has been attributed to the direct process induced by a dc magnetic field of 2 kOe. There are several reports showing that the value of τ for a phonon-bottleneck (PB) process is proportional to T^{-2}. The PB process is a phenomenon in which the magnetic relaxation becomes slow due to energy exchange between the spin system (Gd^{3+}), lattice system, and thermal bath.[33] In the low-temperature region (ac magnetic measurements were performed below 10 K), in which thermal vibrations are suppressed, the mean free path of a low-energy phonon is elongated. In this case, direct coupling between the low-energy phonon and the thermal bath is the dominant heat flow process.[33] In other words, interfacial thermal resistance between the crystal surface and the thermal bath, which depends on the surface and size of the specimen, greatly affects the magnetic relaxation process. Therefore, the simplest way to evaluate the contribution of the PB process is to determine the effects of crystal grinding. Grinding increases the surface area of a crystal as well as the thermal contact between a crystal and the thermal bath, which affects the PB behavior.[16,19,34,35] To validate the effects of crystal size, ac magnetic measurements were performed on pristine crystals of **GdGd** and **GdGd*** (**GdGd$_c$** and **GdGd$_c$***, respectively) in their mother liquor. After the measurements, the pristine crystals were crushed inside the mother liquor, and the ac magnetic susceptibilities were measured again. The χ_M'' versus ν plots for **GdGd$_c$** at 2 and 3 K in a dc field of 2 kOe, in which SR occurs, deviate from the conventional Debye-type relaxation behavior, whereas those for the crushed sample could be fitted by using extended Debye model equations (see Figures S21, S22, and S25 in the Supporting Information). Unusual χ_M'' versus ν curves were observed for the magnetically diluted pristine crystals of **GdGd$_c$*** in a field of 2 kOe. In contrast, the χ_M'' versus ν curves in a field of 200 Oe showed conventional Debye-type behavior (see Figures S23 and S25). The crystal-size-dependent χ_M'' versus ν curves for SR indicate the presence of the PB effect. Therefore, we believe that the BT^2 term in Equation (3) stems from this process.

Table 1. Optimized parameters obtained by using Equations (2) and (3).

FR	ΔE [cm^{-1}]	τ_0 [s]
GdGd*	2.50(3)	$3.66(6)\times10^{-15}$
GdY*	2.2(1)	$6.7(5)\times10^{-5}$
SR	**A [s^{-1}]**	**B [s^{-1}]**
GdGd*	108(4)	14(1)
GdY*	38(2)	13(1)
GdGd	238(7)	22(1)
GdY	79(3)	16(1)

Analysis of ac magnetic susceptibilities

From the dc field dependencies of the dynamic magnetic properties, the Orbach process occurs in a 200 Oe field, whereas PB and direct processes occur in a 2 kOe field. The conversion from FR to SR was observed only under highly diluted conditions (**GdGd***), in which the number of Gd^{3+} ions per 1 nm^3 (n_{Gd}) was 0.044 nm^{-3}. To investigate the n_{Gd} dependence of the dynamic magnetic properties, the ac magnetic susceptibilities were measured for three magnetically diluted samples, which were prepared by doping 25, 50, and 75 mol% **GdGd**

into **YY**; the data are presented in Figure S26 in the Supporting Information. FR was not observed even for the 25 mol% sample ($n_{Gd}=0.11\ nm^{-3}$), whereas SR was observed when the field was >600 Oe. In other words, both FR and SR occur only when $n_{Gd}<0.1\ nm^{-3}$. For spin–lattice relaxations, the energies of the spin systems supplied by ac magnetic fields are transferred to lattice systems. The phonons from spin–lattice relaxations are released to the thermal bath from the surface of the crystals. If the energy of the phonons generated from the spin systems (E_S) is much more than the energy that lattice systems can accept (E_L), the energy exchange between the spin and the lattice systems is inhibited, which results in the lengthening of τ. Because E_S and E_L are proportional to C_{mag} and C_{lat}, respectively, the value of C_{mag}/C_{lat} indicates whether the PB process occurs or not. For **GdGd***, C_{mag}/C_{lat} at 2 K was determined to be 0.76 in a field of 0 Oe, and therefore the lattice system can accept the energy from the spin system. As a result, spin–lattice relaxations (FR) were observed in weak dc fields. However, in a 2 kOe field, C_{mag}/C_{lat} increased to 1.00. In this case, the lattice does not have enough pathways to deal with the energy from the lattice system. As a result, SR was observed in stronger dc fields. Because the triple-decker complexes investigated in this research have 24 butoxy chains per molecule, intermolecular contact in the crystal is inhibited, causing a low Gd^{3+} ion concentration in **GdGd*** and **GdY***. In addition, increasing the strength of the dc magnetic field enhances the energy exchange between the spin and lattice systems, because the number of phonon modes that coincide with the Zeeman splitting energy is proportional to the square of the phonon energy.[33,36] Therefore, saturation of the relaxation pathways, which is essential for the PB process, is induced by applying a strong dc magnetic field. The findings of Marel and co-workers' studies on magnetic relaxations support our hypothesis.[37,38] They suggested that the ac magnetic susceptibilities include spin–lattice relaxations and heat transport between spin systems, lattice systems, and the thermal bath. Their model contains C_{mag}/C_{lat}, which is related to E_S/E_L, and a heat transport coefficient between the spin and lattice systems (α). In their system, a single peak in the χ_M'' versus ν plots was split into two peaks by changing the C_{mag}/C_{lat} and α values. This situation is consistent with the experimental results, in which increasing the applied magnetic field enhances C_{mag} and spin–lattice relaxations (i.e., the direct process). Figure 6a shows the fit of normalized χ_M' and χ_M'' plots (χ' and χ'', respectively) achieved by using the formula [see Eqn. (S3) in the Supporting Information] reported by Marel and co-workers.[37,38] Although they assumed a two-level spin system, which deviates from the situation for the Gd^{3+} complexes, the ac magnetic susceptibilities of **GdGd*** in various dc fields can be reproduced if C_{mag}/C_{lat} and α increase with increasing dc field strength (Figure 6 and Figure S30). The experimental C_{mag}/C_{lat} values derived from the heat capacity measurements changed from 0.76 to 1.00 with an increase in the dc field from 400 to 2 kOe, whereas the values obtained from Marel's equations changed from 0.43 to 1.89. These discrepancies arise from the differences between the two-level system of the model and the multi-level system of the Gd^{3+} complexes.

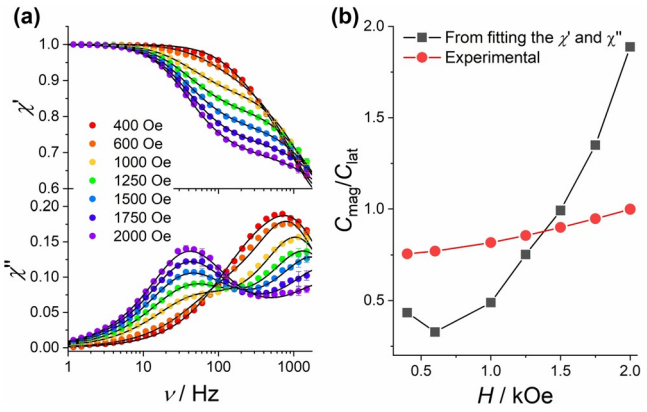

Figure 6. (a) Simulated ac magnetic susceptibilities (solid curves) for **GdGd*** at 1.85 K using Eqn. (S3) in the Supporting Information. χ_M' and χ_M'' were normalized to χ_M' at 1 Hz. (b) Magnetic field dependence of C_{mag}/C_{lat} at 1.85 K derived by fitting the ac magnetic susceptibilities. The experimental values derived from heat capacity measurements are shown for comparison.

Therefore, further improvements to the model are required for a more elaborate analysis.

Conclusions

We have investigated the dynamic magnetic behavior of Gd^{3+} complexes under highly diluted conditions. Undiluted samples underwent a single relaxation process, whereas diluted ones underwent dual relaxation processes. For highly diluted samples, C_{mag} and C_{lat} have the same magnitude, resulting in both PB and spin–lattice relaxation processes, when the applied dc magnetic field has an appropriate strength. For undiluted samples, the magnetic heat capacities are around 10 times larger than the lattice heat capacities, thereby inducing a single magnetic relaxation process attributed to the PB effect. The fit of the ac magnetic susceptibility curves using Marel's model supported our hypothesis. We believe that the phenomena shown here are general for Gd^{3+} complexes under highly diluted conditions ($n_{Gd}\approx10^{-2}\ nm^{-3}$). In addition, we have demonstrated that intramolecular magnetic interactions shortened the τ values. Therefore, our findings show that magnetic dilution reveals spin–lattice relaxations hidden by PB effects, enabling the successive modulation of magnetic relaxation pathways by changing the concentration of the magnetic ions.

Experimental Section

Synthesis of [Gd(obPc)$_2$]

A mixture of 4,5-dibutoxyphthalonitrile (1 g, 3.67 mmol), $[Gd(CH_3COO)_3]\cdot4H_2O$ (182 mg, 044 mmol), and 1,8-diazabicyclo[5.4.0]undec-7-ene (DBU; 0.3 mL) in 1-hexanol (6 mL) was heated at reflux under nitrogen atmosphere for 5 h. After the removal of 1-hexanol under reduced pressure with heating, the residue was purified by column chromatography on silica gel (Wakogel c200) with $CHCl_3$ as the eluent. A deep-green fraction was collected, which was evaporated to dryness. Recrystallization from CH_2Cl_2/methanol gave black crystals (161 mg, 15%). Elemental

analysis (%) calcd for $C_{128}H_{160}N_{16}O_{16}Gd$: C 65.81, H 6.90, N 9.59; found: C 65.79, H 6.88, N 9.70%.

Synthesis of GdGd

$[Gd(obPc)_2]$ (23 mg, 0.0098 mmol), $H_2(obPc)$ (11 mg, 0.010 mmol), and $[Gd(CH_3COO)_3]\cdot 4H_2O$ (20 mg, 0.049 mmol) in 1-hexanol (1.5 mL) was heated at reflux under nitrogen atmosphere for 8 h. After cooling to room temperature, the addition of an excess of methanol gave a violet solid, which was collected by vacuum filtration and washed with methanol. The solid was extracted with CH_2Cl_2 and purified through column of Biobeads S-X1 with tetrahydrofuran as the eluent. A deep-blue fraction was collected, which was evaporated to dryness. Recrystallization from $CHCl_3$/ethanol gave black crystals (19 mg, 54%). Elemental analysis (%) calcd for $C_{192}H_{240}N_{24}O_{24}Gd_2$: C 64.37, H 6.75, N 9.38; found: C 64.36, H 6.92, N 9.36.

Synthesis of YY

$[Y(obPc)_2]$ (23 mg, 0.0098 mmol), $H_2(obPc)$ (30 mg, 0.027 mmol), and $[Y(CH_3COO)_3]\cdot 4H_2O$ (20 mg, 0.059 mmol) in 1-hexanol (3 mL) was heated at reflux under nitrogen atmosphere for 4 h. Following the same purification procedure as used for **GdGd** gave black crystals (54 mg, 58%). Elemental analysis (%) calcd for $C_{192}H_{240}N_{24}O_{24}Y_2$: C 66.92, H 7.02, N 9.76; found: C 66.87, H 7.12, N 9.78.

Synthesis of GdY

$[Gd(obPc)_2]$ (30 mg, 0.013 mmol), $H_2(obPc)$ (30 mg, 0.027 mmol), and $[Y(acac)_3]\cdot xH_2O$ (120 mg, 0.31 mmol) in 1-hexanol (3 mL) was heated at reflux under nitrogen atmosphere for 4 h. Following the same purification procedure as used for **GdGd** gave black crystals (50 mg, 54%). Elemental analysis (%) calcd for $C_{192}H_{240}N_{24}O_{24}Gd_{0.692}Y_{1.308}$: C 66.02, H 6.92, N 9.62; found: C 65.76, H 6.94, N 9.55.

Preparation of GdGd*

GdGd (5.29 mg) and **YY** (59.59 mg) were mixed in $CHCl_3$ (3 mL) and the solution was ultrasonicated for 5 min. Recrystallization by slow diffusion of ethanol gave black crystals (45.82 mg).

Preparation of GdY*

GdY (9.32 mg) and **YY** (43.95 mg) were mixed in $CHCl_3$ (3 mL) and the solution was ultrasonicated for 5 min. Recrystallization by slow diffusion of ethanol gave black crystals (50.00 mg).

Deposition Numbers 1972705 and 1972706 contain the supplementary crystallographic data for this paper. These data are provided free of charge by the joint Cambridge Crystallographic Data Centre and Fachinformationszentrum Karlsruhe Access Structures service www.ccdc.cam.ac.uk/structures.

Acknowledgements

This work was financially supported by the JSPS KAKENHI (Grant nos. JP20225003, JP15K05467, JP24750119, JP14J02656, JP17K19102, and JP18K14242), Tohoku University Molecule and Material Synthesis Platform in the Nanotechnology Platform Project, and CREST, JST (Grant No. JPMJCR12L3). M.Y. thanks the support by the 111 project (B18030) of China. We thank Dr. Y. Nakano for ICP-AES measurements. The scientific grants R-143-000-A80-114 and R-143- 000-A65-133 from the National University of Singapore are gratefully acknowledged. Computational resources from NSCC are gratefully acknowledged. This paper is Contribution No. 61 from the Research Center for Thermal and Entropic Science.

Conflict of interest

The authors declare no conflict of interest.

Keywords: gadolinium · magnetic properties · phonon-bottleneck effect · porphyrinoids · spin–lattice relaxation

[1] R. Sessoli, D. Gatteschi, A. Caneschi, M. Novak, *Nature* **1993**, *365*, 141 – 143.
[2] M. N. Leuenberger, D. Loss, *Nature* **2001**, *410*, 789 – 793.
[3] D. Gatteschi, R. Sessoli, *Angew. Chem. Int. Ed.* **2003**, *42*, 268 – 297; *Angew. Chem.* **2003**, *115*, 278 – 309.
[4] D. N. Woodruff, R. E. Winpenny, R. A. Layfield, *Chem. Rev.* **2013**, *113*, 5110 – 5148.
[5] J. J. Baldoví, S. Cardona-Serra, J. M. Clemente-Juan, E. Coronado, A. Gaita-Arino, H. Prima-García, *Chem. Commun.* **2013**, *49*, 8922 – 8924.
[6] N. Ishikawa, M. Sugita, T. Ishikawa, S.-y. Koshihara, Y. Kaizu, *J. Am. Chem. Soc.* **2003**, *125*, 8694 – 8695.
[7] J. D. Rinehart, J. R. Long, *Chem. Sci.* **2011**, *2*, 2078 – 2085.
[8] F.-S. Guo, B. M. Day, Y.-C. Chen, M.-L. Tong, A. Mansikkamäki, R. A. Layfield, *Science* **2018**, *362*, 1400 – 1403.
[9] C. A. P. Goodwin, F. Ortu, D. Reta, N. F. Chilton, D. P. Mills, *Nature* **2017**, *548*, 439 – 442.
[10] F.-S. Guo, B. M. Day, Y.-C. Chen, M.-L. Tong, A. Mansikkamäki, R. A. Layfield, *Angew. Chem. Int. Ed.* **2017**, *56*, 11445 – 11449; *Angew. Chem.* **2017**, *129*, 11603 – 11607.
[11] Y.-S. Ding, N. F. Chilton, R. E. P. Winpenny, Y.-Z. Zheng, *Angew. Chem. Int. Ed.* **2016**, *55*, 16071 – 16074; *Angew. Chem.* **2016**, *128*, 16305 – 16308.
[12] Y.-C. Chen, J.-L. Liu, L. Ungur, J. Liu, Q.-W. Li, L.-F. Wang, Z.-P. Ni, L. F. Chibotaru, X.-M. Chen, M.-L. Tong, *J. Am. Chem. Soc.* **2016**, *138*, 2829 – 2837.
[13] J. M. Zadrozny, J. Liu, N. A. Piro, C. J. Chang, S. Hill, J. R. Long, *Chem. Commun.* **2012**, *48*, 3927 – 3929.
[14] S. Gómez-Coca, A. Urtizberea, E. Cremades, P. J. Alonso, A. Camón, E. Ruiz, F. Luis, *Nat. Commun.* **2014**, *5*, 4300.
[15] R. Ishikawa, Y. Horii, R. Nakanishi, S. Ueno, B. K. Breedlove, M. Yamashita, S. Kawata, *Eur. J. Inorg. Chem.* **2016**, 3233 – 3239.
[16] L. Tesi, A. Lunghi, M. Atzori, E. Lucaccini, L. Sorace, F. Totti, R. Sessoli, *Dalton Trans.* **2016**, *45*, 16635 – 16643.
[17] T. Yamabayashi, M. Atzori, L. Tesi, G. Cosquer, F. Santanni, M.-E. Boulon, E. Morra, S. Benci, R. Torre, M. Chiesa, L. Sorace, R. Sessoli, M. Yamashita, *J. Am. Chem. Soc.* **2018**, *140*, 12090 – 12101.
[18] M. Atzori, L. Tesi, E. Morra, M. Chiesa, L. Sorace, R. Sessoli, *J. Am. Chem. Soc.* **2016**, *138*, 2154 – 2157.
[19] S. Q. Wu, Y. Miyazaki, M. Nakano, S. Q. Su, Z. S. Yao, H. Z. Kou, O. Sato, *Chem. Eur. J.* **2017**, *23*, 10028 – 10033.
[20] B. Liu, B. Wang, Z. Wang, S. Gao, *Sci. China Chem.* **2012**, *55*, 926 – 933.
[21] M. J. Martínez-Pérez, S. Cardona-Serra, C. Schlegel, F. Moro, P. J. Alonso, H. Prima-García, J. M. Clemente-Juan, M. Evangelisti, A. Gaita-Ariño, J. Sesé, J. van Slageren, E. Coronado, F. Luis, *Phys. Rev. Lett.* **2012**, *108*, 247213.
[22] A. Arauzo, A. Lazarescu, S. Shova, E. Bartolome, R. Cases, J. Luzon, J. Bartolome, C. Turta, *Dalton Trans.* **2014**, *43*, 12342 – 12356.
[23] R. J. Holmberg, L. T. A. Ho, L. Ungur, I. Korobkov, L. F. Chibotaru, M. Murugesu, *Dalton Trans.* **2015**, *44*, 20321 – 20325.
[24] T. Yoshida, G. Cosquer, D. C. Izuogu, H. Ohtsu, M. Kawano, Y. Lan, W. Wernsdorfer, H. Nojiri, B. K. Breedlove, M. Yamashita, *Chem. Eur. J.* **2017**, *23*, 4551 – 4556.

[25] D. C. Izuogu, T. Yoshida, H. Zhang, G. Cosquer, K. Katoh, S. Ogata, M. Hasegawa, H. Nojiri, M. Damjanovic, W. Wernsdorfer, T. Uruga, T. Ina, B. K. Breedlove, M. Yamashita, *Chem. Eur. J.* **2018**, *24*, 9285 – 9294.
[26] K. Katoh, R. Asano, A. Miura, Y. Horii, T. Morita, B. K. Breedlove, M. Yamashita, *Dalton Trans.* **2014**, *43*, 7716 – 7725.
[27] N. F. Chilton, R. P. Anderson, L. D. Turner, A. Soncini, K. S. Murray, *J. Comput. Chem.* **2013**, *34*, 1164 – 1175.
[28] M. Orendáč, L. Sedláková, E. Čižmár, A. Orendáčová, A. Feher, S. A. Zvyagin, J. Wosnitza, W. H. Zhu, Z. M. Wang, S. Gao, *Phys. Rev. B* **2010**, *81*, 214410.
[29] L. F. Chibotaru, L. Ungur, *J. Chem. Phys.* **2012**, *137*, 064112.
[30] F. Aquilante, J. Autschbach, R. K. Carlson, L. F. Chibotaru, M. G. Delcey, L. De Vico, I. F. Galván, N. Ferré, L. M. Frutos, L. Gagliardi, M. Garavelli, A. Giussani, C. E. Hoyer, G. Li Manni, H. Lischka, D. Ma, P. Å. Malmqvist, T. Müller, A. Nenov, M. Olivucci, T. B. Pedersen, D. Peng, F. Plasser, B. Pritchard, M. Reiher, I. Rivalta, I. Schapiro, J. Segarra-Martí, M. Stenrup, D. G. Truhlar, L. Ungur, A. Valentini, S. Vancoillie, V. Veryazov, V. P. Vysotskiy, O. Weingart, F. Zapata, R. Lindh, *J. Comput. Chem.* **2016**, *37*, 506 – 541.
[31] T. Fukuda, N. Shigeyoshi, T. Yamamura, N. Ishikawa, *Inorg. Chem.* **2014**, *53*, 9080 – 9086.
[32] L. Ungur, L. F. Chibotaru, *Phys. Chem. Chem. Phys.* **2011**, *13*, 20086 – 20090.
[33] J. H. Van Vleck, *Phys. Rev.* **1941**, *59*, 724.
[34] D. L. Huber, *Phys. Rev.* **1965**, *139*, A1684.
[35] J. A. Giordmaine, L. E. Alsop, F. R. Nash, C. H. Townes, *Phys. Rev.* **1958**, *109*, 302.
[36] A. M. Stoneham, *Proc. Phys. Soc. London* **1965**, *86*, 1163 – 1177.
[37] T. P. Valkering, L. C. Van Der Marel, *Physica* **1970**, *47*, 412 – 424.
[38] J. Flokstra, G. J. Gerritsma, G. A. Hartemink, L. C. Van Der Marel, *Physica* **1974**, *77*, 99 – 120.

Manuscript received: December 23, 2019
Accepted manuscript online: February 14, 2020
Version of record online: June 5, 2020